Original Article

Plantamajoside modulates the proliferation, stemness, and apoptosis of lung carcinoma via restraining p38MAPK and AKT phosphorylation

Yazhou Li[1,2#], Ruiyang Han[3#], Wei Cao[1^]

[1]Department of Interventional Radiology, The Second Affiliated Hospital of Air Force Medical University, Xi'an 710038, China; [2]Department of Interventional Radiology, BaoJi Hi-Tech People Hospital, Baoji 721000, China; [3]Department of Hepatobiliary and Vascular Surgery, 521 Hospital of the Chinese Weapons Institutes of Health, Xi'an 710065, China

Contributions: (I) Conception and design: W Cao; (II) Administrative support: W Cao; (III) Provision of study materials or patients: Y Li, R Han; (IV) Collection and assembly of data: Y Li, R Han; (V) Data analysis and interpretation: Y Li, R Han; (VI) Manuscript writing: All authors; (VII) Final approval of manuscript: All authors.

[#]These authors contributed equally to this work.

Correspondence to: Wei Cao. Department of Interventional Radiology, The Second Affiliated Hospital of Air Force Medical University, 569 Xinsi Road, Baqiao District, Xi'an 710038, China. Email: cawe001@126.com.

Background: Plantamajoside (PMS), an active anti-inflammatory component and antioxidant derived from *Herba Plantaginis*, has been reported to exert a suppressive effect in liver cancer *in vivo*. In this study, we tested the effects of PMS on the metastatic 95D cell line.

Methods: 95D cells were characterized as most sensitive to PMS across several lung cancer cell lines. Cell viability within 24 h was tested with CCK-8. Different concentrations of PMS (0, 50, 100, and 200 μg/mL) and 5 μg/mL of cisplatin were established for later 24 h treatment. Relative mRNA and protein expression were assessed with PCR and Western blotting. Cell proliferation and stemness were indicated with colony and sphere formation. Cell metastasis was evaluated with wound healing and Transwell. Apoptotic cells and mitochondrial membrane potential were investigated with flow cytometry.

Results: CCK-8 assay showed PMS to inhibit the viability of 95D cells in a dose-dependent manner. PMS decreased colony formation and inhibited stemness in 95D cells. Invasion and migration were also inhibited. Moreover, PMS induced cell apoptosis, and decreased mitochondrial membrane potential. All of these effects were dose dependent. Interestingly, PMS treatment reduced the protein expression of p-p38 MAPK and p-AKT but not that of p38 MAPK and AKT.

Conclusions: PMS inhibited proliferation, stemness, and migration, and initiated apoptosis in 95D cells, possibly through p38 MAPK and AKT dephosphorylation and mitochondria dysfunction. These findings support the promise of PMS as a prodrug in lung cancer treatment.

Keywords: Lung cancer; mitochondrial membrane potential; oxidative stress

Submitted Mar 30, 2020. Accepted for publication Apr 30, 2020.
doi: 10.21037/tcr-20-1834
View this article at: http://dx.doi.org/10.21037/tcr-20-1834

Introduction

Lung cancer is the leading global cause of cancer-related mortality, with non-small cell lung cancer (NSCLC) and small cell lung cancer (SCLC) accounting for roughly 85% and 15% of all incidence, respectively (1). At the time of diagnosis, most patients are already at a late stage of the disease, resulting in a high rate of mortality. Nowadays, new therapeutics like EGFR (epidermal growth factor

^, ORCID: 0000-0002-0841-8247.

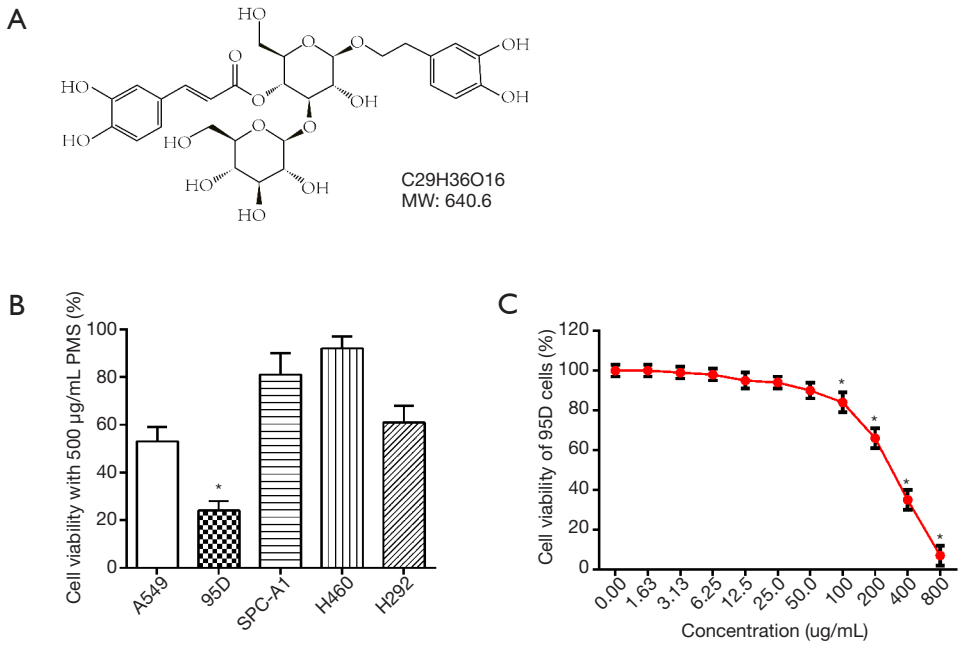

Figure 1 PMS decreased the cell viability of 95D cells. (A) Chemical structure of Plantamajoside (PMS). (B) Cell viability of 95D cells treated with increasing concentrations of PMS. The cells were treated with 0, 1, 2.5, 5, 10, 25, 50, 100, 200, 300, 400, 500, 600, and 800 μg/mL of PMS for 24 h and (C) cell viability was analyzed using Cell Counting Kit 8. The * indicates significant difference ($P<0.05$ compared with other cell lines or untreated 95D cells) by one-way ANOVA or *t*-test.

receptor) inhibitors and immunotherapy offer benefit for lung cancer patients; nevertheless, the 5-year survival rate for patients is less than 20% (2,3). Some signal transduction pathways have been involved in the development of new lung cancer drugs, among which the VEGF, p38 MAPK, and PI3K signaling pathways have proved most attractive. The pathology of NSCLC is usually more closely related to p38 MAPK signaling, while the pathology of SCLC is more closely related to PI3K (4). The need for proper subclassification-based administration is becoming more urgent, and more targeted therapies desperately need to be developed (5).

Plantamajoside (PMS, shown in *Figure 1A*) is the main active ingredient in *Herba Plantaginis*, a conventional TCM. Recently, PMS was shown to be effective against breast cancer in mouse models, exerting an antitumor effect via NF-κB inhibition (6). Later studies revealed the involvement of PI3K/AKT signaling in the activation of NF-κB (7,8). PMS inhibition of PI3K/AKT and NF-κB was also observed in other disease models including lipopolysaccharide (LPS)-induced lung injury, human airway epithelial cell inflammation, and human gingival fibroblasts inflammation (8-10). Meanwhile, other studies have shown PMS-induced NF-κB inhibition to be related to MAPK. As well as being shown to have potential anti-cancer effects through molecular docking with matrix metalloproteinase 2 (MMP-2)/MMP-9 and in mouse models, PMS was also observed in later studies to suppress MMP-1 in a MAPK and NF-κB-dependent way (6,11). In other studies, PMS was shown to inhibit MAPK and NF-κB signaling to prevent LPS-induced lung injury and human umbilical vein endothelial cell dysfunction induced by advanced glycation end-products (9,12). These findings indicated that the mechanism by which PMS inhibits breast cancer could be complex. PMS may also help with the treatment of other tumors based on the widespread pivotal role of p38 MAPK and PI3K/AKT signaling in tumors.

Lung tumors are highly heterogeneous (13), which presents a challenge, not only for diagnosis but also effective treatment. MAPK signaling, which is downstream of several tumor-related pathways, appears to have stimuli-dependent effects. MAPK activation is part of the inflammation and stress signaling involved in tumor progression, and proliferation and senescence (14,15). In general, the inhibition of p38 MAPK, which functions by prohibiting p38 MAPK-induced tumor angiogenesis, is beneficial

for both NSCLC and SCLC patients, with inhibitors of EGFR signaling, in particular, demonstrating widespread clinical benefits (16). SCLC, on the other hand, is often characterized by the loss or mutation of tumor suppressor genes and activation of oncogenes, especially activated PI3K signaling. PI3K activation is mainly thought to promote cell cycle and tumor survival, mainly via AKT activation. PI3K/AKT signaling is also a target of EGFR inhibitors and often induces its drug resistance (17). The limited effectiveness of present drugs, inadequate kinds of therapies referring to lung cancer classification, and the need for personalized therapeutics all call for the discovery and optimization of more targeted anti-cancer drugs.

To objectively assess the antitumor effects of PMS, elementary tasks were performed on the high-metastatic human lung cancer cell line 95D. Cell viability, stemness, apoptosis, oxidative stress, and MAPK and AKT phosphorylation were tested. This study aims to provide new insight into our understanding of the mechanism of the tumor inhibitive effect of PMS, regardless of MMP inhibition.

Methods

Agents

Plantamajoside (PMS) was purchased from CHENGDU MUST BIOTECHNOL CO., LTD (Sichuan, China), purity ≥98%. A549, 95D, SPC-A1, H460 and H292 cells were obtained from the American Type Culture Collection (ATCC; Manassas, VA, USA). RPMI-1640 medium was purchased from HyClone Company (Cat#SH30809.01; Logan, UT, USA). Fetal bovine serum (ATCC 30-2020) was purchased from Thermo Fisher Scientific (MA, USA). Dimethyl sulfoxide (DMSO), 1-bromo-3-chloropropane, Isopropanol, ethanol, cisplatin (DDP) and other solvents were obtained from Sigma (St. Louis MO, USA). Cell Counting Kit-8 (CCK-8), 0.25% trypsin, 0.01 M PBS (powder, pH7.2–7.4), 1% Paraformaldehyde, Mitochondrial Membrane Potential Assay Kit with JC-1, and 100× Penicillin-Streptomycin Solution were bought from Beijing Solarbio Science & Technology Co., Ltd. (Beijing, China). B27, epidermal growth factor (EGF) and basic fibroblast growth factor (bFGF) were purchased from Invitrogen (CA, USA). Primary antibodies, including anti-Caspas-3 (Cat#ab13847), anti-Caspas-9 (Cat#ab32539), anti-SOX2 (Cat#ab93689), anti-CD44 (Cat#ab216647), anti-OCT4 (Cat#ab19857), anti-Bax (Cat#ab32503), anti-Bcl-2 (Cat#ab32124), anti-MAPK (Cat#ab32062), anti-p-MAPK (Cat#ab247405), anti-AKT (Cat#ab32505) and anti-p-AKT (Cat#ab81283) were purchased from Abcam (Cambridge, MA, USA). Anti-GAPDH (Cat#60004-1-lg) and all secondary antibodies were bought from PTG Company (Rosemont, IL, USA). Trizol, BeyoRT™ III First Strand cDNA Synthesis Kit with gDNA EZeraser, PCR Kit with Taq, Total Superoxide Dismutase Assay Kit with WST-8, Lipid Peroxidation MDA Assay Kit, Annexin V-FITC/PI apoptosis kit, Crystal Violet Staining Solution, and others were purchased from Beyotime Biotechnology (Shanghai, China).

Cell culture and viability

Cells were cultured in RPMI-1640 medium with 10% FBS and 1% Penicillin-Streptomycin solution at 37 ℃ with 5% CO_2, before being digested with 0.25% trypsin and stored at –80 ℃ in FBS with 10% DMSO. A549, 95D, SPC-A1, H460, and H292 cells were treated with 500 μg/mL PMS before viability were tested. The viability of 95D cells under treatment of different concentrations of PMS, was further explored. Cells with 80% confluence were digested and seeded into 96-well plates at a density of 1×10^4 cells/well in 100 μL medium. Different concentrations of PMS were obtained by mixing medium and an 800 mg/mL PMS stock solution, which was prepared with PMS dissolved in culture medium (1 mg:1.25 mL). Solutions of certain concentrations in 100 μL medium were added to the wells 24 h after seeding. Three replicates were made for each concentration. The solutions were left for 24 h incubation. An hour before the OD_{450} value was read, 20 μL of CCK-8 was added to each well.

Colony formation assay

Properly re-suspended cells were randomly plated into 6-well plates at a density of 1×10^4 cells/well in 1 mL culture medium. Then, medium with 0, 50, 100, or 200 μg/mL PMS was added. Triplicated wells were used for each group. To avoid PMS hydrolysis, the culture mediums with different concentrations of PMS were refreshed every 24 h. Cell debris and unattached cells were washed away, and fresh medium without PMS was added after 36 h, followed by incubation for 10 days. The attached cells were then stained with 0.1% (W/V) crystal violet.

Table 1 Primers used in PCR

Gene	Forward primer 5'-3'	Reverse primer 5'-3'
Ki67	GCCCCTAAAGTAGAACCCGT	GGGTTCGGATGATTTGCCTC
PCNA	CGGATACCTTGGCGCTAGTA	CACTCCGTCTTTTGCACAGG
Survivin	GTCCCTGGCTCCTCTACTG	GACGCTTCCTATCACTCTATTC
GAPDH	GAGTCAACGGATTTGGTCGT	TTGATTTTGGAGGGATCTCG

mRNA extraction and cDNA preparation

Each group of cells (approximately 1×10^6 cells) was incubated in a 6-cm plate for 24 h, then cultured with medium containing 0, 50, 100, or 200 μg/mL PMS for a further 24 h. After thorough washing with cold PBS, 1 mL of Trizol was added to wash out the plate and the solution was collected. The solution was then added with 200 μL of 1-bromo-3-chloropropane, vortexed, and incubated for 5 min at room temperature. The supernatant was collected after centrifugation under 13,000 rpm for 15 min at 4 ℃. Next, isopropanol (500 μL) was added and incubated for 5 min at room temperature, the mixture was centrifuged under 13,000 rpm for 10 min at 4 ℃ and the RNA pellets were collected. Then, the pellets were incubated with 1 mL of 70% ethanol and centrifuged at 7,500 rpm for 10 min at 4 ℃. The liquid was subsequently discarded, and the pellets were air dried. The RNA pellets were dissolved with DNase/RNase-free water, and the RNA concentration was tested. Finally, first-strand cDNA was synthesized according to the manufacturer's instructions.

Polymerase chain reaction (PCR)

The synthesized cDNA (2 μL), 10× PCR Buffer (with Mg^{2+} 2 μL), dNTP (2.5 mM each, 1.6 μL), primer mix (10 μM each, 1.6 μL), Taq DNA Polymerase (5 U/μL, 0.1 μL), and pure water (12.7 μL) were mixed and incubated at 94 ℃ for 3 min. Then, 30 cycles of incubation were applied at 94 ℃ for 30 sec, 55 ℃ for 30 sec, and 72 ℃ 60 sec. At the end of the cycle, the mixture was kept at 72 ℃ for an additional 10 min. DNA agarose gel electrophoresis was then performed to show the relative expression of specific genes. The primers used are listed in *Table 1*.

Sphere formation assay

To analyze sphere formation, 95D cells were seeded in ultra-low attachment 24-well culture plates at 2×10^3 cells per well, and incubated under serum-free conditions in RPMI 1640 containing 20 μL/mL of B27, 20 ng/mL of EGF, 20 ng/mL of bFGF, and 1% penicillin-streptomycin. After 10 days of incubation at 37 ℃ with 5% CO_2, pictures were taken under a microscope and the number of spheres was counted in 3 separate 40× fields.

Western blotting

For Western blotting analysis, 95D cells were seeded at a density of 2×10^6 cells/well in 6-well plates. When confluence was acceptable, the cells were washed and medium with 0, 50, 100 or 200 μg/mL PMS was randomly added to each well. After 24 h of incubation, the cells were washed out with cold PBS, lysed, and checked by Bradford assay. In SDS-PAGE, about 40 μg of protein was used for each sample. The primary and secondary antibodies were incubated according to the protocols of the manufacturers. The proteins of interest were visualized by enhanced chemiluminescence reagents with ChemiDoc XRS.

Wound healing

Wound-healing assay was performed to evaluate the migration of 95D cells. Briefly, Cells were seeded in 6-well plates to reach 90% confluence. Then, straight scratches were created with a sterile pipette tip. The destroyed cells were gently rinsed off with PBS 3 times and cultured in medium. Then, wound healing was imaged at 0 and 24 h with a digital camera (Leica DFC300FX) equipped inverted microscope.

Transwell

Transwell invasion was tested with chambers with Matrigel (1 mg/mL) (Becton-Dickinson, New Jersey, USA) according to the manufacturer's instructions. Briefly, 200 μL serum-free medium containing 1×10^5 cells/well was added into the

upper chamber, and the lower chamber contained 0.6 mL medium containing 20% FBS. After 24 h, the cells on the upper chamber were removed. The lower chamber cells were fixed and stained with crystal violet.

Flow cytometry

To study apoptosis, flow cytometry was performed according to the manufacturer's protocol. In brief, 95D cells treated with different doses of PMS were fixed with 4% paraformaldehyde for 30 min at 4 ℃, collected, and re-suspended in PBS. Then, the cells were incubated with Annexin V-FITC for 15 min and with PI for 10 min. The cells were analyzed with a FACScan flow cytometer (BD Biosciences, Franklin Lakes, NJ, USA).

For analysis of mitochondrial potential, cells were digested, centrifuged, and then re-suspended with JC-1 working solution. The cells were then incubated at 37 ℃ with 5% CO_2 for 15 min, and centrifuged and re-suspended once more in PBS. Finally, analysis was carried out with FACScan.

SOD and MDA activity tests

Cells were washed twice with ice cold PBS, scratched, and collected in cold PBS. Next, the cells were homogenized and centrifuged under 600 g for 15 min at 4 ℃, and the supernatants were collected. Protein concentrations were then tested by Bradford assay, with about 50 μg of proteins used for each sample. The samples, Wst-8/enzyme working solution, reaction initiating solution, and PBS were added according to protocol, and incubated at 37 ℃ for 30 min. Optical density was then tested under 450 nm.

For MDA activity assay, cell lysates were harvested and tested using BCA KIT as in Western blotting. According to the protocol, MDA testing working solution was prepared, optical density under 532 nm was tested, and MDA concentration was corrected using curve of the standard.

Statistical analysis

Statistical analyses were performed with Graphpad Prism 6.0 (GraphPad Software, Inc., La Jola, CA, USA). Data were analyzed by one-way ANOVA or Student's *t*-test, and were expressed as mean ± standard deviation (SD). Statistical significance was represented by $P<0.05$.

Results

PMS dose-dependently suppressed the survival of 95D lung cancer cells

To observe the influence of PMS on lung cancer cells and to establish proper treatment doses for subsequent experiments, cell viability was tested by CCK-8 assay. Among a series of lung cancer cell lines, 95D cells seemed most sensitive to 500 μg/mL PMS treatment and was used in later experiments (*Figure 1B*). Under treatment of PMS for 24 h, cell viability decreased in a dose-dependent manner (*Figure 1C*). Cells treated with 100 μg/mL of PMS began to exhibit significantly lower viability than the control group. To test the mechanism of action by which PMS hindered lung carcinoma, treatments with 0, 50, 100, and 200 μg/mL of PMS were established and 5 μg/mL of DDP was introduced as positive control in the following experiments.

PMS suppressed proliferation of 95D lung cancer cells

To further validate the effect of PMS on 95D cell proliferation, crystal violet staining was carried out to count the number of colonies. As shown in *Figure 2A*,*B*, when compared with the control group, treatment with 100 and 200 μg/mL of PMS significantly inhibited colony formation in 95D cells. Colony formation was very significantly inhibited by 200 μg/mL of PMS, possibly because of toxicity-related cell death. Subsequently, the mRNA expressions of proliferation marker Ki67, PCNA, and survivin were detected by reverse transcription PCR and were all clearly decreased with 100 or 200 μg/mL of PMS. These results showed dose-dependent suppression of proliferation of 95D cells by PMS.

Anti-stem cell activity of PMS in 95D lung cancer cell culture

Spheroid formation assay was then applied. As shown in *Figure 3A*,*B*,*C*, 100 and 200 μg/mL of PMS significantly reduced the spheres in both diameter and number compared with the control group. Further testing was performed for stem cell markers SOX-2, CD44, and OTC. With the increase of PMS concentration, SOX-2, CD44. and OTC were all reduced in a dose-dependent manner, as shown in *Figure 3D*,*E*. These results showed that PMS reduced the

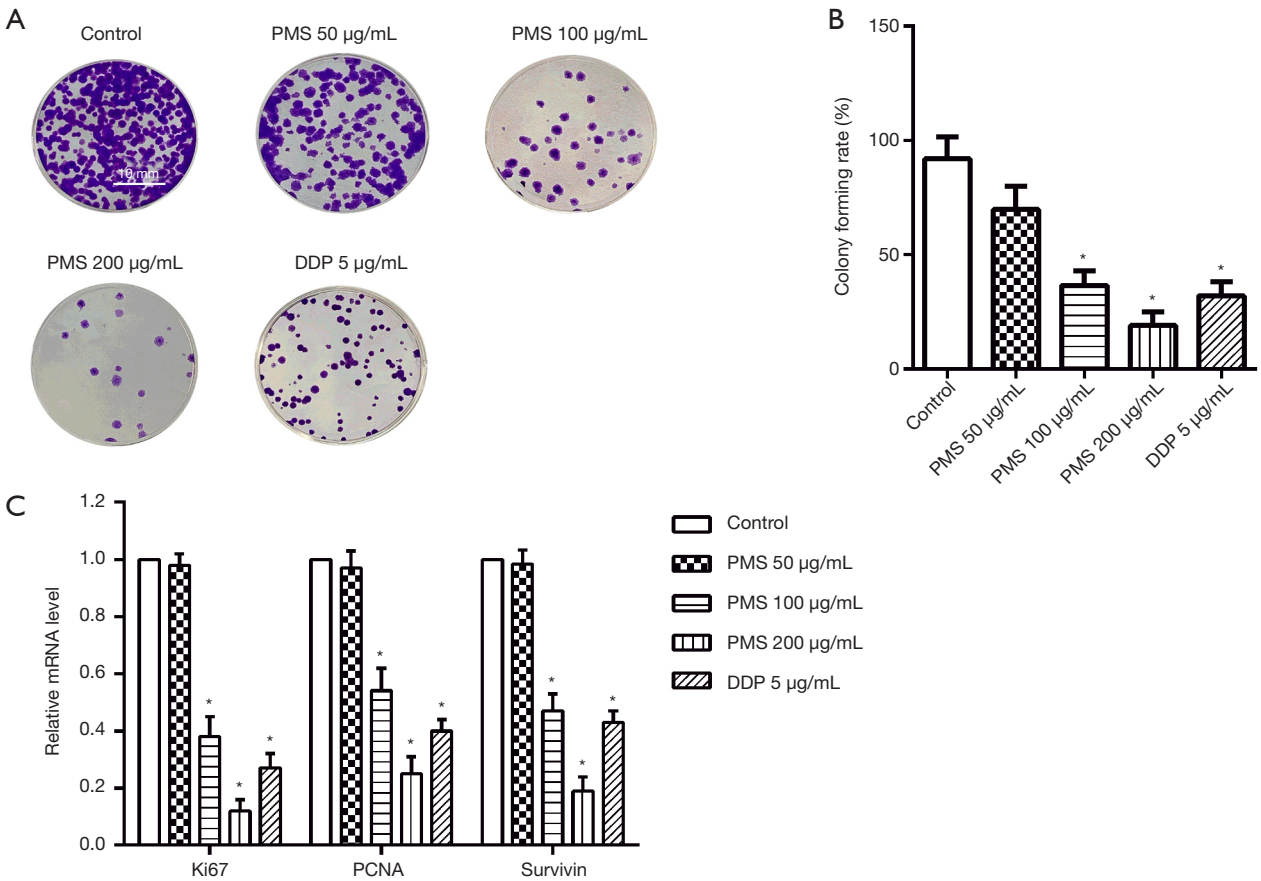

Figure 2 Dose-dependent reduction of 95D cell proliferation by PMS. (A and B) Reduced colony formation rate by PMS of 0, 50, 100, and 200 μg/mL for 2 weeks. (C) Relative mRNA expression of proliferative markers Ki67, PCNA, and survivin. 95D cells were treated with 0, 50, 100, and 200 μg/mL of PMS for 24 h. Data are shown as mean ± SEM from at least three replicates, *P<0.05 compared with the control group.

stemness of 95D cells dose dependently.

PMS inhibited invasion and metastasis of 95D lung cancer cells (Figure 4)

The invasion and metastasis of 95D cells were then evaluated. Treatment with 100 μg/mL of PMS significantly suppressed wound enclosure (*Figure 4A*,*C*). Invasive cells tested with Transwell were also reduced with 100 and 200 μg/mL of PMS (*Figure 4B*,*D*). The results indicated that PMS inhibited the invasion and metastasis of 95D cells.

PMS promoted apoptosis of 95D lung cancer cells

Cell apoptosis was then assessed using the Annexin V-FICT/PI apoptosis detection kit. PMS dose-dependently induced 95D cell apoptosis (*Figure 5A*), with significant apoptosis seen at 100 μg/mL. The number of apoptotic cells was further elevated at 200 μg/mL of PMS. The protein expressions of caspase-3 and caspase-9 were tested by Western blotting (*Figure 5B*). Both cleaved caspase-3 expression and cleaved caspase-9 expression increased in a dose-dependent manner relative to the control group. Treatment with 100 μg/mL of PMS was enough to induce effective apoptosis, and this was more significant with 200 μg/mL of PMS. These results showed that PMS treatment induces apoptosis in 95D cells.

PMS reduced lung cancer cell 95D mitochondrial membrane potential

Mitochondrial membrane potential is the direct energy

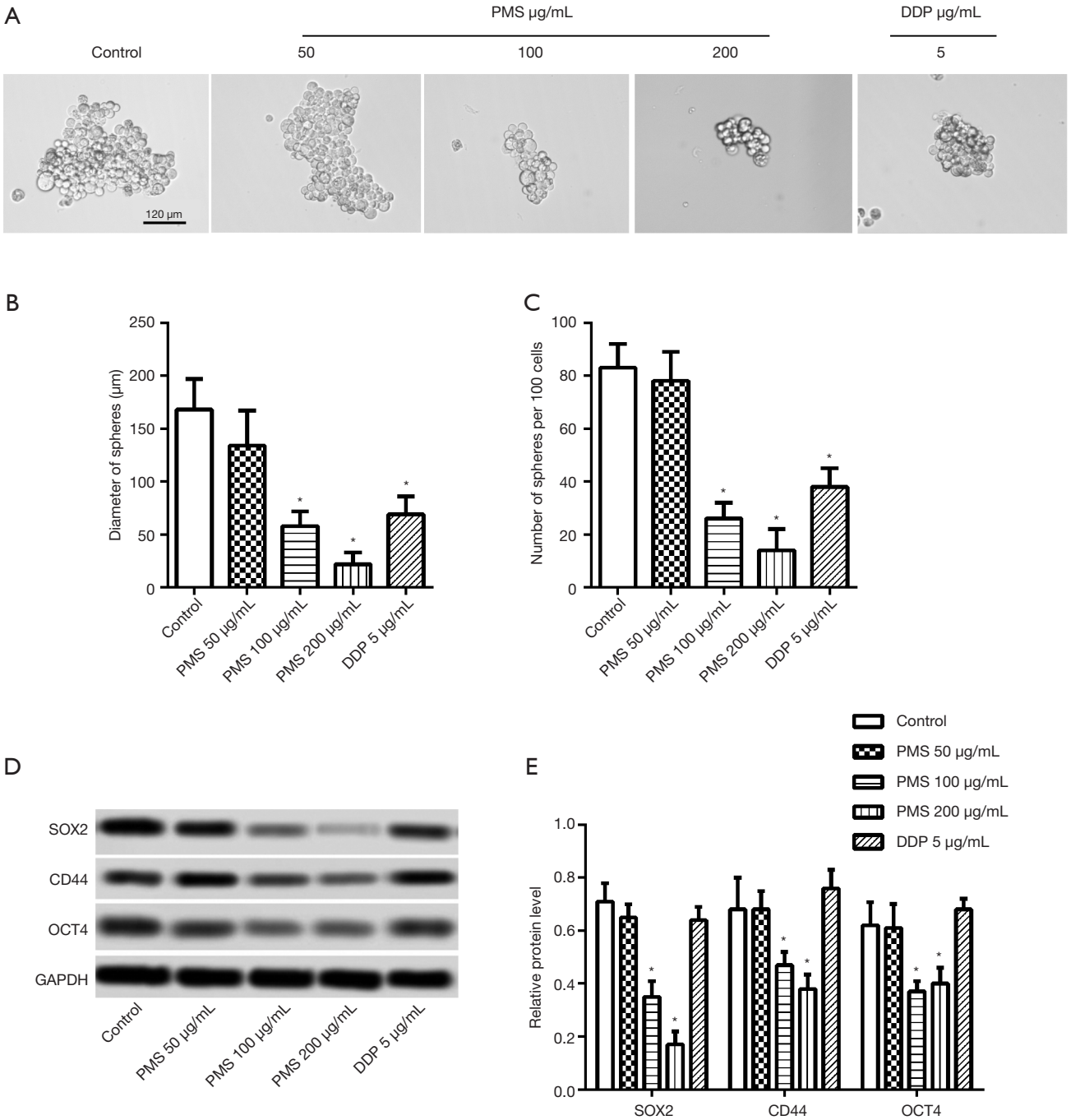

Figure 3 Anti-stem cell activity of PMS in 95D cultures. (A) Spheroid formation was tested to characterize the stemness of 95D cells under treatment of PMS (0, 50, 100, and 200 μg/mL) for 10 days , the diameter (B) and number (C) of spheres were then measured. (D) Stemness markers SX-2, CD44, and OTC4 were measured by Western blotting. (E) Relative protein levels of SX-2, CD44, and OTC4 were quantified with Image J and presented in bar graphs. Data are shown as mean ± SEM from at least three replicates, *P<0.05 compared with the control group.

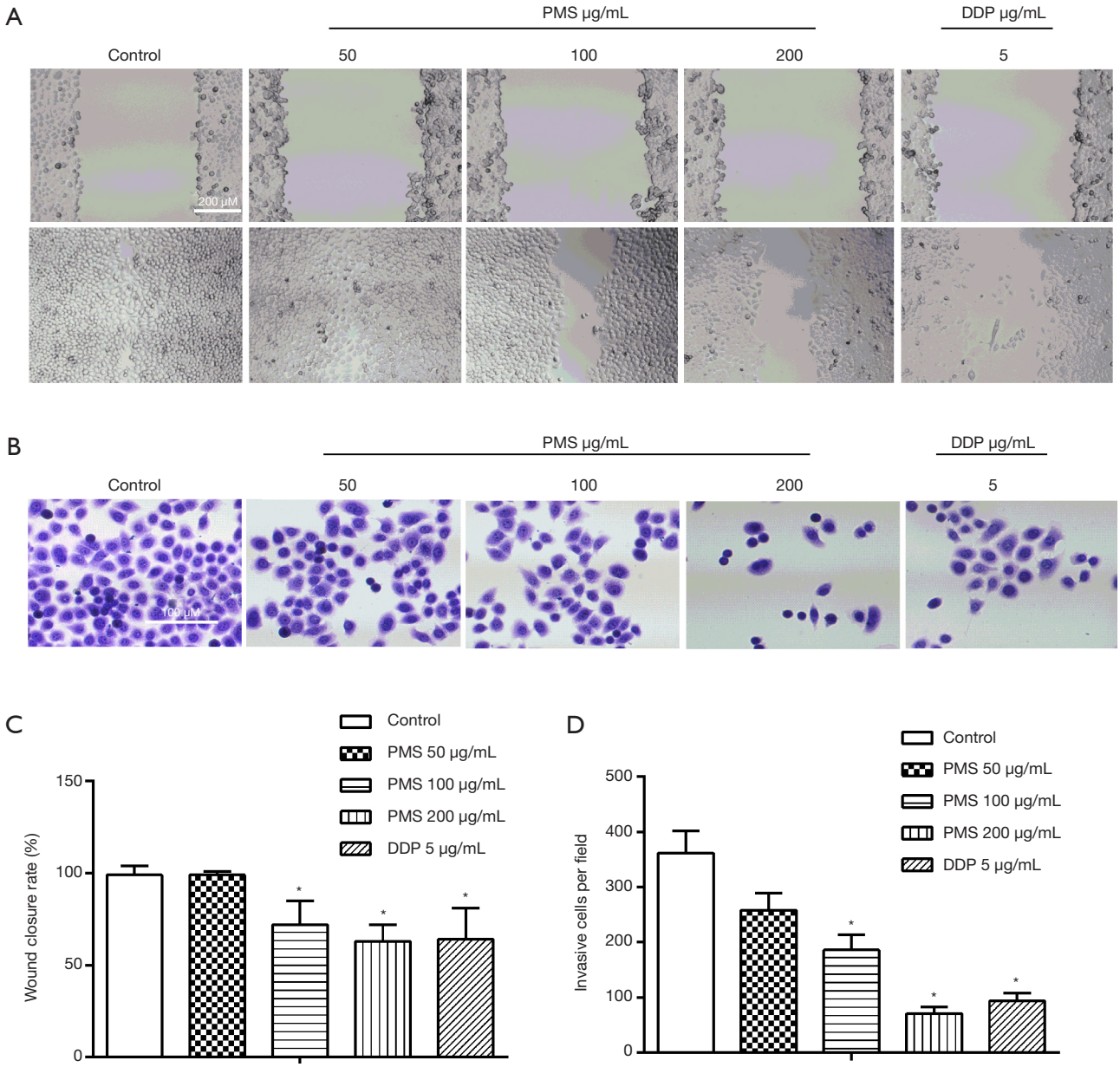

Figure 4 PMS inhibited metastases and migration in 95D cells. (A) Wound enclosure of 95D cells tested with wound healing assay. (B) Invasive 95D cells tested with Transwell. The wound enclosure (C) and invasive cells (D) were quantified with Image J and analyzed with *t*-test. Data are shown as mean ± SEM from at least three replicates, *P<0.05 compared with the control group.

source of ATP synthase. Reduced mitochondrial membrane potential, accompanied by oxidative stress, is usually seen and tested in apoptotic tumor cells (18). Here, mitochondrial membrane potential was measured using JC-1. Under normal conditions, mitochondrial membrane potential is high, JC-1 accumulates in the mitochondria matrix, and red fluorescence is observed; when the mitochondrial membrane potential turns low, JC-1 disperses, and green fluorescence is observed. Flow cytometry showed a dose-dependent increase in JC-1 green fluorescence, which indicated decreased mitochondrial membrane potential (*Figure 6A*).

Bax and Bcl-2 are, respectively, important positive and negative regulators of mitochondrial membrane

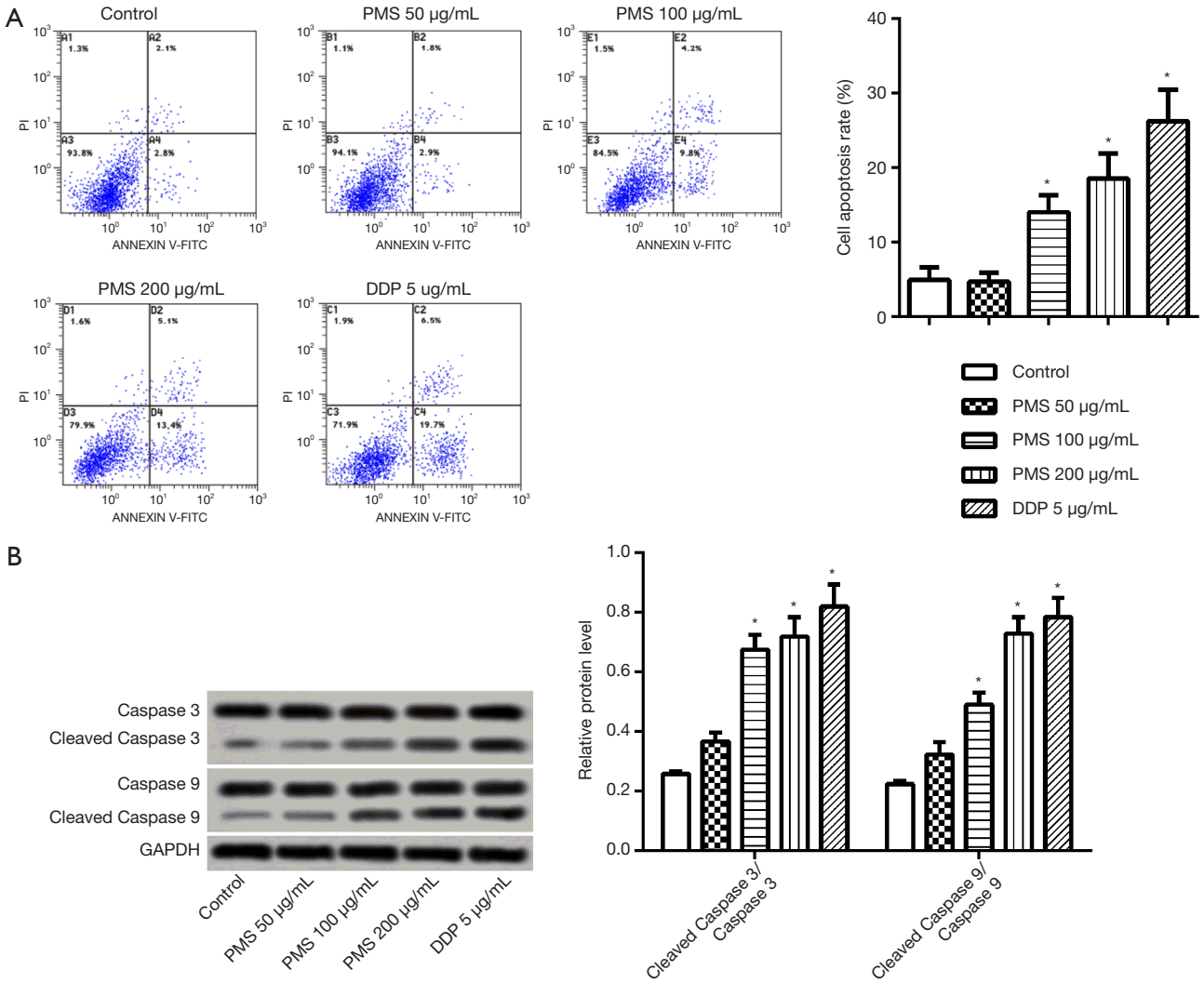

Figure 5 PMS induced apoptosis in 95D cells. (A) Apoptosis in PMS (0, 50, 100, and 200 μg/mL)-treated 95D cells for 24 h. (B) Relative protein expression of cleaved caspase 3 and cleaved caspase 9 to caspase 3 and caspase 9, respectively. Data are shown as mean ± SEM from at least three replicates, *P<0.05 compared with the control group.

permeability. The Bax/Bcl-2 ratio is an important adaptor of apoptosis (19). As the PMS concentration increased, the protein expression of Bax rose and that of Bcl-2 decreased (*Figure 6B*). Under 50 μg/mL of PMS treatment, the Bax/Bcl-2 ratio was significantly increased compared with the control group. Moreover, a more dramatic increase of Bax/Bcl-2 was observed in cells treated with 100 and 200 μg/mL of PMS.

Mitochondria was then isolated and SOD and MDA were measured (*Figure 6C,D*) to assess the impact of PMS on 95D cell oxidative stress. Under treatment of 100 and 200 μg/mL of PMS, SOD was significantly decreased *vs.* the control group, and MDA was significantly increased.

Taken together, these results indicated the involvement of mitochondria in PMS-induced apoptosis, possibly through decreased mitochondrial membrane potency and increased oxidative stress.

Phosphorylation of p38 MAPK and AKT is suppressed in PMS treated 95D lung cancer cell

The mechanism by which PMS suppressed survival

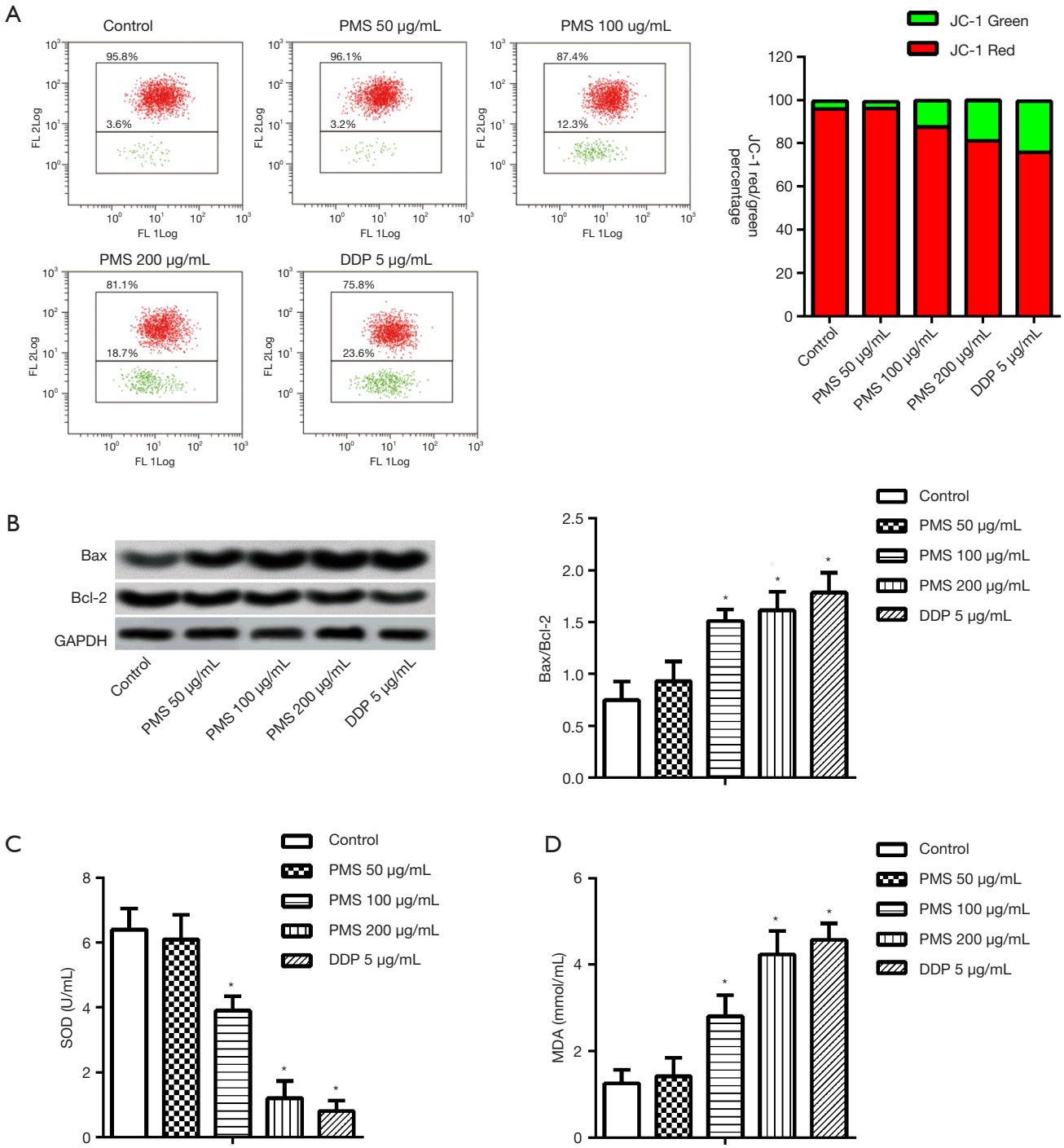

Figure 6 PMS reduced mitochondrial membrane potential in 95D cells. (A) PMS (0, 50, 100, and 200 μg/mL) treatment for 24 h reduced 95D cell mitochondrial membrane potential characterized by JC-1 labeled flow cytometry. (B) Relative expression of apoptosis proteins Bax to Bcl-2, and reduced expression of SOD (C) and increased amount of MDA (D) were tested. Data are shown as mean ± SEM from at least three replicates, *P<0.05 compared with the control group.

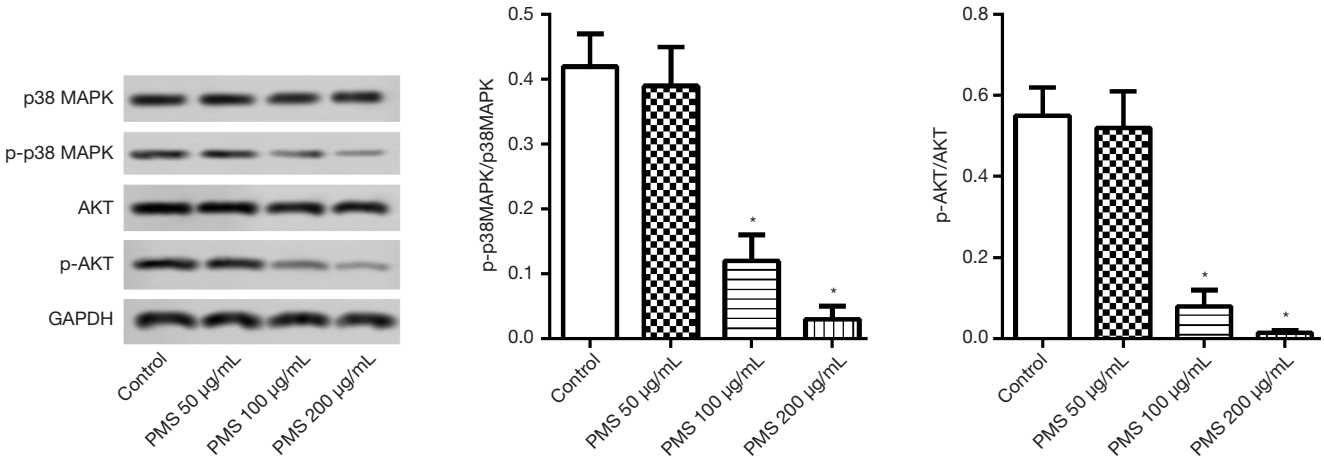

Figure 7 Suppressed phosphorylation of p38 MAPK and AKT in PMS-treated 95D cells. PMS (0, 50, 100, and 200 μg/mL) treatment for 24 h. Relative protein expression of p38 MAPK, p-p38 MAPK, AKT, and p-AKT was tested. Data are shown as mean ± SEM from at least three replicates, *P<0.05 compared with the control group.

and proliferation, and promoted apoptosis in 95D cells was further explored. AKT and p38 MAPK and their phosphorylated forms were detected (*Figure* 7). There was no significant change in p38 MAPK or AKT; however, less phosphorylated p38 MAPK and AKT were seen. These results implied that the antitumor effects of PMS involve the inhibition of AKT and p38 MAPK.

Discussion

Traditional Chinese medicines are excellent sources of innovative antitumor drugs. Many formulas, herbal extracts, and monomers are attributed with antitumor properties or can provide effective adjuvant therapy in cancer treatment (20,21). The characterization and optimization of natural compounds have always been important steps in the discovery anti-cancer drugs. PMS possesses antiviral, diuretic, antioxidant, and immune enhancement potential (22). Several years ago Pei *et al.* showed the anti-cancer effect of PMS in MDA-MB-231 human breast cancer cells and in 4T1 cell allograft mice (6). Li *et al.* showed that PMS suppressed LPS-induced NF-κB and IL-6 in esophageal squamous cell carcinoma cells (ESCC), thus inhibiting epithelial-mesenchymal transition (EMT) in ESCC (7). However, in vivo, the structure of PMS is far from stable. According to a pharmacokinetics study of PMS in rats, PMS was absorbed soon after administration but was completely eliminated within 6 h (23). When its numerous hydroxyls and esters are considered, this is structurally understandable (*Figure 1A*), and the distribution of this highly water-soluble structure into tumor targets could not be expected to occur easily. Taking this into account, it was remarkable that PMS achieved a significant difference in mice . Here, we showed that PMS exerted a dose-dependent inhibitory effect on 95D cell viability. Little influence was observed with PMS concentrations of less than 50 μg/mL, which can possibly be explained by the strong hydrolysis of PMS. PMS activity in 95D cells is not as strong as that in MDA-MB-231 or ESCC (6,7), possibly because curing lung cancer presents a bigger challenge. These studies strongly supported PMS as a promising prodrug.

Both inhibited proliferation and stemness are important indicators of antitumor activity; however, no previous studies had explored this in relation to PMS before. In the present study, we showed that PMS treatment dose-dependently inhibited the proliferation and stemness of 95D cells in vitro. This indicated that PMS may exert its antitumor effect through other undiscovered mechanism of actions beyond MMP and NF-κB inhibition.

Mitochondria plays a pivotal role in cancer, especially in the supply of energy and biosynthetic precursors, ROS production, and apoptosis. Mitochondria-related apoptosis is the most common downstream mechanism of antitumor agents, the process of which has been shown to decrease mitochondrial membrane potency, increase homodimers of Bax, and accumulate ROS, leading to caspase cleavage and apoptosis-related cell death (18,19). In this study,

we showed that PMS treatment resulted in decreased mitochondrial membrane potency, accumulated ROS and Bax, and increased cleaved caspase 3/9 in 95D cells (*Figures 4* and *5*). These results strongly suggested that PMS treatment induces mitochondria-related cell apoptosis in lung carcinoma.

PI3K/AKT and p38 MAPK are two important pathways in the regulation of tumorigenesis, cell cycle, metastasis, drug resistance, and survival in lung cancer, and represent two main tumor targets (24-26). AKT phosphorylation is an important way in which PI3K is activated, resulting in cell cycle progression and the inhibition of apoptotic signaling (17). Meanwhile, P38 MAPK can be activated or inactivated upon treatment with different antitumor agents, and usually leads to stimuli-dependent effects (15). The inactivation of p38 MAPK has been evidenced to induce apoptosis, which is part of the mechanism of action of VEGFR inhibitors (25). Our results showed that under treatment of PMS, AKT expression remained the same, while AKT phosphorylation decreased remarkably. At the same time, PMS reduced p-p38 MAPK but not p38 MAPK expression. These results indicated the involvement of PI3K/AKT and p38 MAPK signaling in PMS-induced apoptosis in 95D cells.

AKT and p38 MAPK-induced apoptosis has usually been observed in antitumor therapeutics. Flupentixol, for instance, could be specifically docked to PI3K to inhibit the PI3K/AKT pathway and survival of lung cancer cells (27). Meanwhile, torilis japonica extract induced apoptosis by reducing the mitochondrial membrane potential via the regulation of the AMPK-p38 MAPK signaling pathway (28), and Paris Saponin I enhanced apoptosis by influencing the p38 MAPK, ERK, and Akt pathways in lung cancer cells (4). Both Akt and p38 MAPK are involved in a large number of antitumor activities, and sometimes, both are involved. Some authors have suggested that co-inhibition of AKT and MAPK might prove effective in avoiding drug resistance (29), while others believe MAPK inhibition weakens the outcome of anticarcinogens (24). In any case, it is clear that these two signaling pathways promote apoptosis. Considering the fact that PMS is easily hydrolyzed but performed well in the present study, proper structural modifications could achieve unexpected effects.

In conclusion, in a dose-dependent manner, PMS treatment inhibited cell viability and proliferation, limited stemness, decreased mitochondrial potential, increased oxidative stress, and activated apoptosis in 95D cells, possibly by inhibiting AKT and p38 MAPK phosphorylation.

Acknowledgments

Funding: This study was supported in part by the Natural Science Foundation of Shaanxi Province (No.2016SF-108). The funders had no role in the study design, data collection and analysis, decision to publish, or preparation of the manuscript.

Footnote

Data Sharing Statement: Available at http://dx.doi.org/10.21037/tcr-20-1834

Conflicts of Interest: All authors have completed the ICMJE uniform disclosure form (available at http://dx.doi.org/10.21037/tcr-20-1834). All authors report grants from Natural Science Foundation of Shaanxi Province (No.2016SF-108), outside the submitted work.

Ethical Statement: The authors are accountable for all aspects of the work in ensuring that questions related to the accuracy or integrity of any part of the work are appropriately investigated and resolved.

References

1. Torre LA, Bray F, Siegel RL, et al. Global cancer statistics, 2012. CA Cancer J Clin 2015;65:87-108.
2. Shankar A, Dubey A, Saini D, et al. Environmental and occupational determinants of lung cancer. Transl Lung Cancer Res 2019;8:S31-49.
3. Osmani L, Askin F, Gabrielson E, et al. Current WHO guidelines and the critical role of immunohistochemical markers in the subclassification of non-small cell lung carcinoma (NSCLC): Moving from targeted therapy to immunotherapy. Semin Cancer Biol 2018;52:103-9.

4. Liu Z, Zheng Q, Chen W, et al. Chemosensitizing effect of Paris Saponin I on Camptothecin and 10-hydroxycamptothecin in lung cancer cells via p38 MAPK, ERK, and Akt signaling pathways. Eur J Med Chem 2017;125:760-9.
5. Wang Q, Shen B, Qin X, et al. Akt/mTOR and AMPK signaling pathways are responsible for liver X receptor agonist GW3965-enhanced gefitinib sensitivity in non-small cell lung cancer cell lines. Transl Cancer Res 2019;8:66-76.
6. Pei S, Yang X, Wang H, et al. Plantamajoside, a potential anti-tumor herbal medicine inhibits breast cancer growth and pulmonary metastasis by decreasing the activity of matrix metalloproteinase-9 and -2. BMC Cancer 2015;15:965.
7. Li X, Chen D, Li M, et al. Plantamajoside inhibits lipopolysaccharide-induced epithelial-mesenchymal transition through suppressing the NF-kappaB/IL-6 signaling in esophageal squamous cell carcinoma cells. Biomed Pharmacother 2018;102:1045-51.
8. Liu F, Huang X, He JJ, et al. Plantamajoside attenuates inflammatory response in LPS-stimulated human gingival fibroblasts by inhibiting PI3K/AKT signaling pathway. Microb Pathog 2019;127:208-11.
9. Wu H, Zhao G, Jiang K, et al. Plantamajoside ameliorates lipopolysaccharide-induced acute lung injury via suppressing NF-kappaB and MAPK activation. Int Immunopharmacol 2016;35:315-22.
10. Ma C, Ma W. Plantamajoside Inhibits Lipopolysaccharide-Induced MUC5AC Expression and Inflammation through Suppressing the PI3K/Akt and NF-kappaB Signaling Pathways in Human Airway Epithelial Cells. Inflammation 2018;41:795-802.
11. Han AR, Nam MH, Lee KW. Plantamajoside Inhibits UVB and Advanced Glycation End Products-Induced MMP-1 Expression by Suppressing the MAPK and NF-kappaB Pathways in HaCaT Cells. Photochem Photobiol 2016;92:708-19.
12. Son WR, Nam MH, Hong CO, et al. Plantamajoside from Plantago asiatica modulates human umbilical vein endothelial cell dysfunction by glyceraldehyde-induced AGEs via MAPK/NF-kappaB. BMC Complement Altern Med 2017;17:66.
13. de Sousa VML, Carvalho L. Heterogeneity in Lung Cancer. Pathobiology 2018;85:96-107.
14. del Barco Barrantes I, Nebreda AR. Roles of p38 MAPKs in invasion and metastasis. Biochem Soc Trans 2012;40:79-84.
15. Fang Y, Wang J, Wang G, et al. Inactivation of p38 MAPK contributes to stem cell-like properties of non-small cell lung cancer. Oncotarget 2017;8:26702-17.
16. Cristea S, Sage J. Is the Canonical RAF/MEK/ERK Signaling Pathway a Therapeutic Target in SCLC? J Thorac Oncol 2016;11:1233-41.
17. Perez-Ramirez C, Canadas-Garre M, Molina MA, et al. PTEN and PI3K/AKT in non-small-cell lung cancer. Pharmacogenomics 2015;16:1843-62.
18. Burke PJ. Mitochondria, Bioenergetics and Apoptosis in Cancer. Trends Cancer 2017;3:857-70.
19. Edlich F. BCL-2 proteins and apoptosis: Recent insights and unknowns. Biochem Biophys Res Commun 2018;500:26-34.
20. Jiang Y, Liu LS, Shen LP, et al. Traditional Chinese Medicine Treatment as Adjuvant Therapy in Completely Resected Stage IB-IIIA Non-Small-Cell Lung Cancer: Study Protocol for a Multicenter, Double-Blind, Randomized, Placebo-Controlled Trial. Clin Lung Cancer 2019;20:e541-7.
21. Wang XQ, Zhang Y, Hou W, et al. Association between Chinese Medicine Therapy and Survival Outcomes in Postoperative Patients with NSCLC: A Multicenter, Prospective, Cohort Study. Chin J Integr Med 2019;25:812-9.
22. Doan DD, Nguyen NH, Doan HK, et al. Studies on the individual and combined diuretic effects of four Vietnamese traditional herbal remedies (Zea mays, Imperata cylindrica, Plantago major and Orthosiphon stamineus). J Ethnopharmacol 1992;36:225-31.
23. Bai L, Han L, Lu X, et al. UHPLC-MS/MS determination and pharmacokinetic study of plantamajoside in rat plasma after oral administration of single plantamajoside and Plantago asiatica extract. Biomed Chromatogr 2017. doi: 10.1002/bmc.3883.
24. Wang J, Li J, Cao N, et al. Resveratrol, an activator of SIRT1, induces protective autophagy in non-small-cell lung cancer via inhibiting Akt/mTOR and activating p38-MAPK. Onco Targets Ther 2018;11:7777-86.
25. Zhang S, Fu Y, Wang D, et al. Icotinib enhances lung cancer cell radiosensitivity in vitro and in vivo by inhibiting MAPK/ERK and AKT activation. Clin Exp Pharmacol Physiol 2018. [Epub ahead of print].
26. Wu Y, Zhang Y, Liu C, et al. Amplification of USP13 drives non-small cell lung cancer progression mediated by AKT/MAPK signaling. Biomed Pharmacother 2019;114:108831.
27. Dong C, Chen Y, Li H, et al. The antipsychotic agent

flupentixol is a new PI3K inhibitor and potential anticancer drug for lung cancer. Int J Biol Sci 2019;15:1523-32.
28. Kim GT, Lee SH, Kim YM. Torilis japonica extract-generated intracellular ROS induces apoptosis by reducing the mitochondrial membrane potential via regulation of the AMPK-p38 MAPK signaling pathway in HCT116 colon cancer. Int J Oncol 2016;49:1088-98.
29. Sato H, Yamamoto H, Sakaguchi M, et al. Combined inhibition of MEK and PI3K pathways overcomes acquired resistance to EGFR-TKIs in non-small cell lung cancer. Cancer Sci 2018;109:3183-96.

Cite this article as: Li Y, Han R, Cao W. Plantamajoside modulates the proliferation, stemness, and apoptosis of lung carcinoma via restraining p38MAPK and AKT phosphorylation. Transl Cancer Res 2020;9(6):3828-3841. doi: 10.21037/tcr-20-1834

